

Landslides (2014) 11:29–42
 DOI 10.1007/s10346-012-0370-4
 Received: 22 May 2012
 Accepted: 9 November 2012
 Published online: 13 December 2012
 © Springer-Verlag Berlin Heidelberg 2012

J. A. Fernández-Merodo · J. C. García-Davalillo · G. Herrera · P. Mira · M. Pastor

2D viscoplastic finite element modelling of slow landslides: the Portalet case study (Spain)

Abstract This paper proposes a hydro-geomechanical finite element model to reproduce the kinematic behaviour of large slow landslides. The interaction between solid skeleton and pore fluids is modelled with a time dependent $u-p_w$ formulation and a groundwater model that takes into account recorded daily rainfall intensity. A viscoplastic constitutive model based on Perzyna's theory is applied to reproduce soil viscous behaviour and the delayed creep deformation. The proposed model is applied to Portalet landslide (Central Spanish Pyrenees). This is an active paleo-landslide that has been reactivated by the construction of a parking area at the toe of the slope. The stability analysis reveals that, after the constructive solutions were undertaken, the slope is in a limit equilibrium situation. Nevertheless, time-dependent analysis reproduces the nearly constant strain rate (secondary creep) and the acceleration/deceleration of the moving mass due to hydrological changes. Overall, the model reproduces a 2-m displacement in the past 8 years that coincides with in situ monitoring data. The proposed model is useful for short- and mid-term predictions of secondary creep. However, long-time predictions remain uncertain, stability depends strongly on the position of the water table depth and new failures during tertiary creep due to soil temporal microstructural degradation are difficult to calibrate.

Keywords Slow landslides · Viscoplasticity · Creep · Biot theory · Finite elements

Introduction

Slow-moving landslides are a widespread type of active mass movement that cause severe damages to infrastructures and may be a precursor of sudden catastrophic slope failures. In this context, modelling slow-moving landslide behaviour is an important task in order to quantify and reduce the risk associated to this geological process. Two broad categories of models can be distinguished to predict landslide mobility: the phenomenological models and the physically based models. The first category employs empirical relationships, statistical or probabilistic approaches and artificial neural networks to relate soil movements and their causes. The latter provides relationships taking into account the mechanical soil behaviour. A summary of the different methods proposed in the literature can be found in Federico et al. (2004).

Physically based models have been mostly used in practical cases to estimate landslide occurrence and stability conditions for a given scenario through a stability factor based on limit equilibrium analysis. Apart from earthquake studies, time-dependent analysis is requested when: (1) hydrological conditions change as in the case of rainfall; (2) resistant parameters are reduced as in the case of strain softening or weathering processes; and (3) creep behaviour is taken into account. Therefore, modelling time evolution of real landslides is a difficult task if we take into account all these different aspects. Complex numerical models as the finite element method can provide a good understanding of the

mechanism of failure because they can reproduce the fully coupled hydrogeological and mechanical behaviour. Moreover, advanced constitutive laws, complex 3D geometries and spatial variations in soil properties can be used. Many numerical modelling case studies of landslides mechanics have already been published focusing on one of these aspects: hydro-mechanical coupling (Tacher et al. 2005; François et al. 2007), strain localisation (Dounias et al. 1988; Troncone 2005) and viscoelastoplasticity (Desai et al. 1995; Vulliet 2000). However, very few studies implement several factors at the same time.

Several landslides affect the Portalet area located on the upper Tena Valley (Central Spanish Pyrenees). Mobilised materials are mainly made of Devonian and Carboniferous materials, characterised by an intense weathering and a high plasticity. In the summer of 2004, the slope excavation at the foot of the slope carried out to build a parking area reactivated two existing paleo-landslides generating a new sliding surface, located 7–16 m below the surface. Measured displacements performed with differential Global Positioning System (GPS) and a ground-based synthetic aperture radar (SAR) system revealed that the moving mass was still active after the constructive solutions were undertaken. Recent underground investigation of Portalet landslide including in situ and laboratory tests and advanced remote monitoring techniques has been carried out in order to better understand the landslide kinematics (Herrera et al. 2011). A simple 1D infinite slope viscoplastic model was first proposed by Herrera et al. (2009). This model assumes that the slip surface shear strength is at residual conditions taking into account recorded daily rainfall. The dissipation of the excess pore fluid is introduced through a consolidation equation. This simple model is very sensible to any variation of the parameters limiting the conclusions that can be drawn from infinite slope models. A second model based on a 2D elastoplastic finite element analysis was proposed by Fernández-Merodo et al. (2008). In this study, the transient analysis is not able to reproduce measured displacements, i.e., no deformation was predicted during long dry time periods, indicating that viscous phenomena and delayed deformation due to creep plays a fundamental role in the landslide kinematics.

These viscous phenomena are now well recognised from laboratory conditions. However, the links with practical applications are almost not existent. For this reason, this paper aims to improve such numerical analysis proposing a 2D viscoplastic finite element model that overcomes these limitations and reproduces Portalet landslide kinematics.

The outline of the paper is as follows. In the first section, the main features of Portalet landslide and available monitoring data are recalled. The proposed complete model (mathematical, constitutive and numerical) for slow landslide is then presented. The mathematical model describes the hydro-mechanical coupling through Biot equations. Creep and viscous mechanical behaviours of soil are introduced in the context of Perzyna's theory. The mathematical and constitutive models are then implemented in a numerical model based on the finite element method. The numerical simulations of

the Portalet landslide are presented in a third section. Stability of the initial and excavated configurations of the slope are firstly analysed. Then, time-dependent numerical simulations are carried out taking into account viscoplasticity and the pore-pressure fluctuations due to rainfall. Finally, conclusions arise from the comparison between the computed kinematics and the monitoring data.

The Portalet landslide

Geomorphological and geological description

The study area is located in the upper part of the Gállego River valley in the Central Spanish Pyrenees (Sallent de Gállego, Huesca) close to the Formigal ski resort. This is a structurally complex area, outcrops of Paleozoic material of Gavarnie mantle were affected by the Hercynian folding phases and the alpine tectonics. Pyrenean deglaciation and widespread structural relaxation shaped the landscape triggering complex landslides that have been previously described and mapped by various authors (Bixel et al. 1985; García Ruiz et al. 2004). We focus our work on two of these landslides developed on the southwest-facing hillside of Petrasos Peak: the “Portalet landslide” and “Petruso landslide” (zones 1 and 2 in Fig. 1). These landslides are rotational slide earth flows, 30–50 m thick. The mobilised materials involve sands and gravels found within a clayey matrix with sandstone levels, greywackes and shales. A subsequent third earth flow can be recognised in the north part of the Portalet landslide (zone 3 in Fig. 1). Nowadays, rock falls (zone 7 in Fig. 1) and avalanches (zone 8 in Fig. 1) are still occurring in the main scarps. Recent small landslides triggered by river erosion can also be found on the toe of the main landslides (zone 9 in Fig. 1).

In summer 2004, the excavation of the foot of the slope carried out to build a parking area (purple line in Fig. 1) reactivated the existing slide surfaces generating a new small earth slide called the “Parking landslide” (zone 11 in Fig. 1), 380 m long and 290 m wide (0.065 km²). The occurrence of this new local landslide prevented the digging to be finished and affected the connection road to France. Constructive solutions were carried out to stabilise the hillside involving re-profiling of the landslide toe, building of small retaining walls and drainage systems. However, field observations indicate that the landslide is still moving. Figure 2 shows the main scarps in the upper part of the slope and the bulging at the toe. This paper concentrates on this landslide studying profile AA' defined in Fig. 1.

Geophysical and geotechnical campaigns were carried out in 2009 and 2010 in order to deeper characterise the geometry and the hydro-geomechanical behaviour of the Portalet landslide. Cross-section profiles were obtained with electrical and seismic tomography; seven new boreholes were performed; and three inclinometers and three piezometers with continuous real time records were installed. According to installed inclinometers the main slip surface of Parking landslide is located at 12 m in borehole S1 (Fig. 1).

The geological cross-section of Parking landslide (Fig. 1) shows four levels: the superficial level (L1) is formed by colluvium material, mainly gravels, sands and sandy-clayey silts with limestone boulders. Immediately below a level (L2) of silt and sandy clay with gravel size fragments appears. The next level (L3) is composed by fragmented slate with a lower degree of weathering. Finally, the substrate (L4) is mainly composed by non-altered slate

and occasionally by boards of tectonised limestone.

The geomechanical characterisation was carried out through in-situ and laboratory tests. SPT tests were performed each 1.5 m in seven boreholes. A total of 42 identification tests (grain size distribution, density, water content, Atterberg limits), 5 direct shear tests and 18 unconfined compression tests were done in undisturbed samples. Results of the tests in the colluvium (level L1) and altered soil (level L2) were not very reliable, due to the heterogeneity of the grain size in the colluvium and the degree of alteration in the slate material. Additional in situ shear tests using a cylindrical hydraulic cell (Oviedo University 2011) were also performed in excavated trenches in order to overcome this inconvenience (Álvarez-Fernández and González-Nicieza 2011). The obtained geomechanical mean properties of the materials are presented in Table 1. More details of the geomechanical characterisation can be found in (ARCO TECNOS 2010).

Monitoring description

Concerning monitoring of the landslide kinematics, seven total station campaigns at 17 ground control points were performed between December 2004 and March 2005, after the toe excavation and the local rupture. During this period, a maximum total displacement of 51 cm was observed in 102 days (1820 mm/year). Inclinometers readings were performed between May and October 2005, indicating that the slip surface was located between 7 and 16 m. In inclinometer S-1 the rupture surface was detected at a depth of 12 m, measuring a displacement of 8 cm in 74 days (365 mm/year) before the total failure of the inclinometer (Fig. 3).

After the stabilisation solutions were carried out in the landslide, five differential GPS (precise DGPS) campaigns were performed between May 2006 and July 2007, measuring a maximum displacement of 530 mm/year (Fig. 4a) denoting a deceleration process. Coinciding with the DGPS campaigns performed between September and November 2006, a ground based SAR has been installed on a hill overlooking the Parking landslide, measuring up to 1,184 mm/year (Herrera et al. 2009). An additional DGPS campaign was performed in October 2011 to complete the monitoring data, which yielded a 360 mm/year maximum displacement rate between May 2006 and October 2011 (Fig. 4b).

In order to complement this measurements, advanced DInSAR processing of satellite SAR images from ERS and Envisat satellites (2001–2007) and TerraSAR-X satellites (2008) were also performed (Herrera et al. 2011). Unfortunately, Parking landslide velocity was too fast to be detected with SAR satellites. However, we were able to measure up to 97 mm/year beyond the crown of this landslide in 2008 from TerraSAR-X satellite images. Concerning the rest of Portalet landslide deposit, far away from the Parking landslide area of influence, satellite measurements reveal a very slow/stable 14 mm/year velocity, which is in agreement with available DGPS measurements (Fig. 4b).

The measurements obtained with the different monitoring techniques (SAR, DGPS, and inclinometers) are described in Herrera et al. (2009, 2011). In these works, the comparison between GB-SAR and DGPS reveals a 7.7 ± 7.4 mm error.

Landslide classification and activity

Many systems have been proposed for the classification of landslides (Fell et al. 2000), but only three of them are considered within this work. Varnes' (1978) landslide classification is based

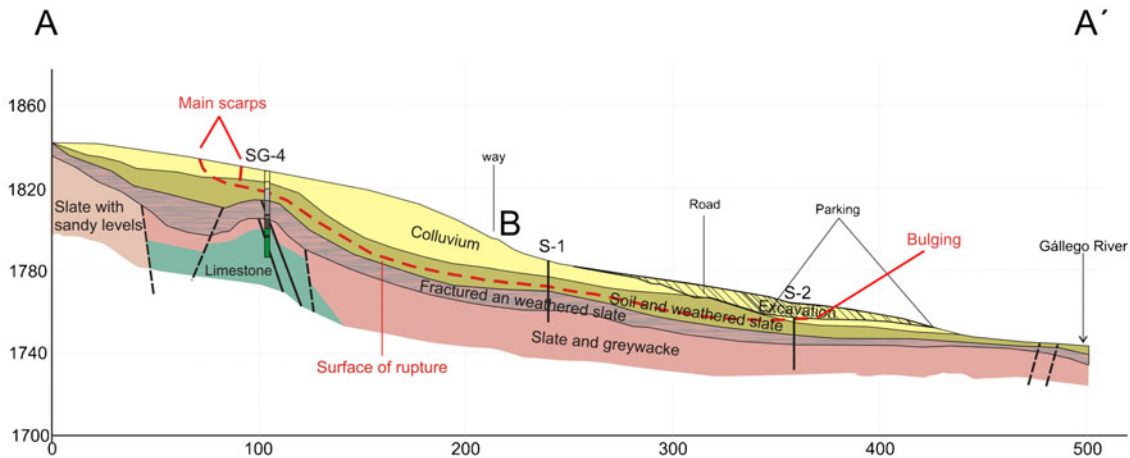
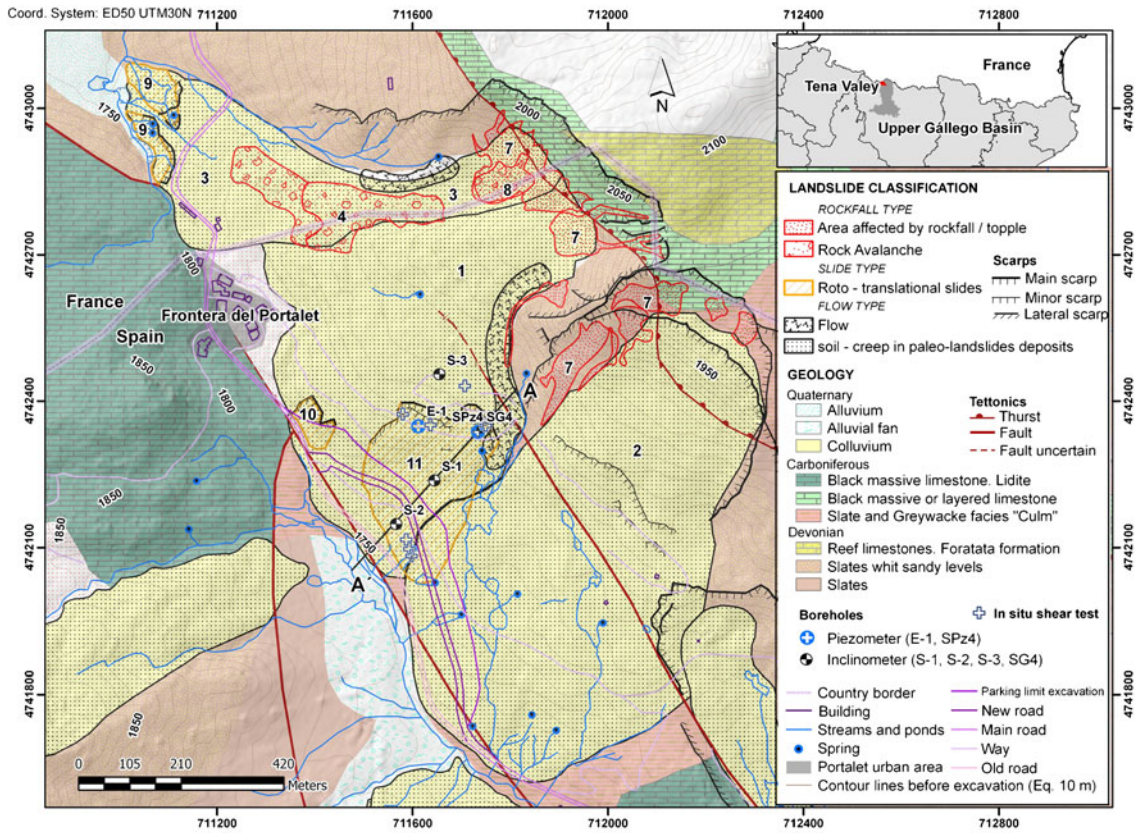


Fig. 1 Geomorphological and geological sketch of the Portalet landslides area and cross-section AA' of the Portalet parking landslide

on: the material type and the type of movement. As it has been pointed out in the geomorphological description, many kinds of slope movements have been identified in the Portalet area. The Portalet landslide can be classified as "complex" with combination of two or more principal types of movement. In this work, we focus on the Parking earth slide (zone 11 in Fig. 1) that affects the lower part of Portalet landslide deposit (zone 1 in Fig. 1).

If we take into account the landslide velocity classification proposed by Cruden and Varnes (1996), we observe that according to measured displacements the Portalet landslide (zone 1 in Fig. 1) is extremely slow and the Parking landslide (zone 11 in Fig. 1) is very slow. Measured displacements showed

farther two kinematic patterns. The first one corresponds to a constant strain rate patterns that has been interpreted as creep by Herrera et al. (2011). In creep mechanics, one can differentiate between three stages: the primary, secondary and tertiary creep stages. These terms correspond to a decreasing, constant and increasing creep strain rate, respectively. The second pattern corresponds to an hydraulic effect (interstitial water pressure changes). Herrera et al. (2009) have shown that the Portalet landslide reacts almost immediately to daily rainfall. This rapid response is likely due to the drainage capacity of the colluvium deposit located on top and to the presence of superficial cracks and preferential drainage pathways.

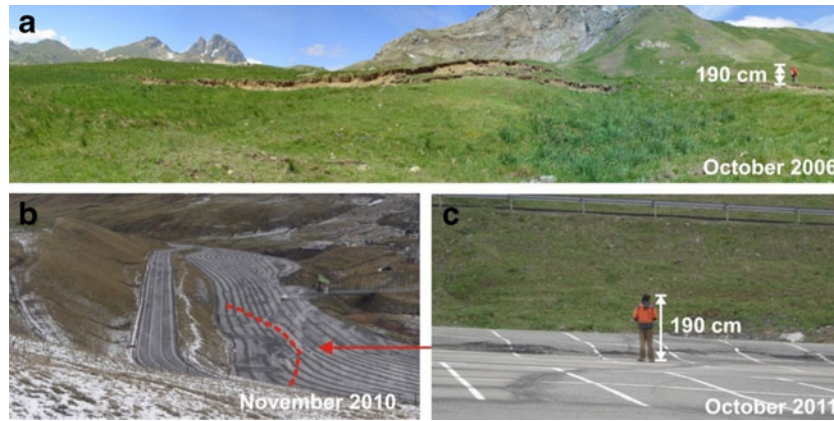


Fig. 2 Portalet parking landslide. **a** Main scarps in the upper part of the slope. **b** Bulging at the toe. **c** Detail of the bulging at the toe

Finally, Leroueil et al. (1996) classification system can give a deeper explanation of landslide state and history. According to these authors landslides undergo, during their life, four stages: the pre-failure stage, the failure stage, the post-failure stage and, eventually, the reactivation stage. Within the latter stage, controlled by localised shear and creep along pre-existing slip surfaces, a phenomenon is defined as active if there is a moving landslide body. The kinematic patterns of the Portalet paleo-landslide previously described can perfectly fit in this last stage, where the excavation of the toe in summer of 2004 and the subsequent local Parking failure correspond to the occasional reactivation event.

In the following sections, the described and interpreted landslide behaviour will be reproduced using the proposed mathematical, constitutive and numerical models.

Landslide modelling

Mathematical model: formulation of the time dependent hydro-geomechanical coupling

In order to achieve a realistic representation of the landslide behaviour, the first requisite is to use a suitable mathematical model to describe the main physical processes taking place within the considered materials, chiefly the interaction between the solid skeleton (the soil grains) and the pore fluids (water and air). The equations of dynamic poro-elasticity due to Biot have been extended and modified by Zienkiewicz and co-workers (e.g. in Zienkiewicz and Shiomi 1984) in order to broaden their scope and ease their implementation within numerical models.

The model included in this study is the so-called u - p_w formulation described by Zienkiewicz et al. (1999), which expresses the governing equations in terms of only two variables, namely the displacements \mathbf{u} of the solid matrix and the pressure p_w of the pore fluid. These equations, which do not consider convective terms and are based on the assumption of negligible relative accelerations between solid and fluid, can be summarised as follows:

1. Balance of linear momentum for the solid–fluid mixture

$$\mathbf{S}^T (\boldsymbol{\sigma}' - \mathbf{m} p_w) + \rho_m \mathbf{b} = \rho_m \ddot{\mathbf{u}} \quad (1)$$

where $\boldsymbol{\sigma}'$ is the vectorial form of the effective stress tensor, vector \mathbf{m} represents the second-order Kronecker-delta, ρ_m is the mass density of the solid–fluid mixture, \mathbf{b} is the vector of body forces per unit mass, $\ddot{\mathbf{u}}$ is the acceleration of the solid skeleton and \mathbf{S} the vectorial form of the strain operator.

2. Combination of the equations for fluid mass conservation and fluid linear momentum balance

$$\mathbf{m}^T \mathbf{S} \dot{\mathbf{u}} - \nabla^T (\mathbf{k}_w \nabla p_w) + \frac{\dot{p}_w}{Q^*} + \nabla^T \mathbf{k}_w \rho_w \mathbf{b} = \mathbf{o} \quad (2)$$

where \mathbf{k}_w is the permeability matrix, Q^* is the coupled volumetric stiffness of solid grains and fluid and ρ_w is the specific weight of the pore fluid.

Table 1 Geomechanical mean properties of the materials

Material	ρ (kg/m ³)	E (kN/m ²)	ν	φ (°)	c' (kN/m ²)
Colluvium deposit (L1)	2,100	1.95×10^4	0.3	30	10
Altered slate–Soil (L2)	2,170	1.95×10^4	0.3	24–20	10
Fragmented slate (L3)	2,170	4×10^4	0.28	23	173
Intact slate (L4)	2,770	4×10^6	0.2	31	640

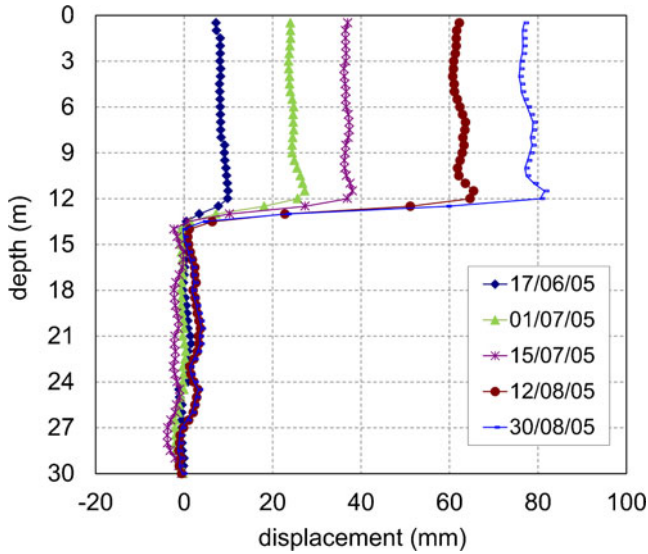


Fig. 3 Inclinometer S-1 measurements

3. A suitable constitutive equation for the soil skeleton (see section below)

$$d\sigma' = D_{ep} \cdot d\varepsilon \quad (3)$$

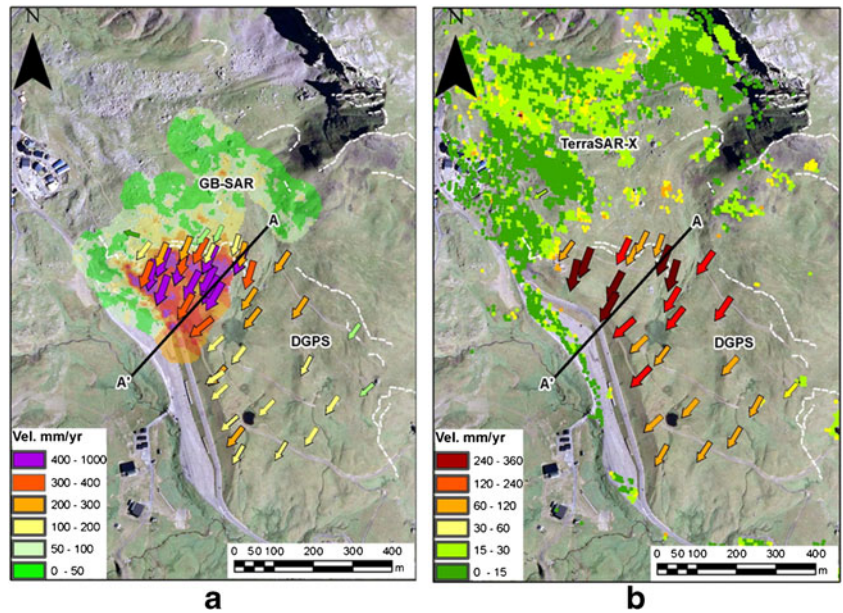
where D_{ep} is the constitutive operator, and ε is the strain vector.

4. Kinematic relationships between displacements and strains assuming small strains

$$d\varepsilon = S \cdot du \quad (4)$$

Finally, an appropriate set of boundary and initial conditions in terms of u and p_w needs to be introduced in order to define completely the problem under consideration.

Fig. 4 Deformation monitoring of the Portalet landslide. a GB-SAR (colored pixels) and DGPS (arrows) between May 2006 and July 2007. b TerraSAR-X (colored pixels) and DGPS (arrows) between May 2006 and October 2011 (Orthophotomap courtesy of Instituto Geográfico Nacional)



Numerical model: finite element discretisation

The continuous partial differential equations presented above can be converted to ordinary differential equations in a discrete form using standard Galerkin techniques (see for instance Zienkiewicz and Taylor 2000). Introducing two appropriate sets of shape functions N_u and N_p for the spatial interpolation of the displacement and pressure fields ($u = N_u \bar{u}$ and $p_w = N_p \bar{p}_w$) the u - p_w formulation results on:

$$\begin{aligned} M \ddot{\bar{u}} + \int_{\Omega} B^T \sigma' d\Omega - Q \bar{p}_w &= f_u \\ Q^T \dot{\bar{u}} + H \bar{p}_w + C \dot{\bar{p}}_w &= f_p \end{aligned} \quad (5)$$

where the matrix B is the discrete form of the strain operator; the matrices M , C , Q and H stand for the usual mass, compressibility, coupling and permeability terms, respectively; and f_u and f_p are the contributing forces (see for instance Zienkiewicz et al., 1999).

A simplification is obtained when the accelerations are neglected, which is the consolidation form:

$$\begin{aligned} \int_{\Omega} B^T \sigma' d\Omega - Q \bar{p}_w &= f_u \\ Q^T \bar{u} + H \bar{p}_w + C \dot{\bar{p}}_w &= f_p \end{aligned} \quad (6)$$

Finally, the static and steady state form is obtained if the variations with respect to time are assumed to be very small:

$$\begin{aligned} \int_{\Omega} B^T \sigma' d\Omega - Q \bar{p}_w &= f_u \\ H \bar{p}_w &= f_p \end{aligned} \quad (7)$$

Employing a generalised Newmark scheme for the time discretisation, a non-linear system of equations with discrete variables (in both time and space) can be obtained out of the equations above. Then, for the computation of every time-step Δt , the non-linear system of equations can be solved iteratively using an appropriate algorithm, typically of the

Newton–Raphson type, which results in the following linear system of equations:

$$\begin{bmatrix} \mathbf{M} + \frac{1}{2}\Delta t^2\beta_2\mathbf{K}_T & -\theta\Delta t\mathbf{Q} \\ \beta_1\Delta t\mathbf{Q}^T & \theta\Delta t\mathbf{H} + \mathbf{C} \end{bmatrix}_{(i)} \begin{bmatrix} \delta(\Delta\ddot{\mathbf{u}}) \\ \delta(\Delta\dot{\mathbf{p}}_w) \end{bmatrix}_{(i+1)} = - \begin{bmatrix} \Phi_u \\ \Phi_p \end{bmatrix}_{(i)} \quad (8)$$

where the tangent stiffness matrix \mathbf{K}_T is given by

$$\mathbf{K}_T = \int_{\Omega} \mathbf{B}^T \mathbf{D}_{ep} \mathbf{B} d\Omega \quad (9)$$

The constants β_1 , β_2 and θ are the parameters of the Newmark scheme for time integration. The vectors $\delta(\Delta\ddot{\mathbf{u}})$ and $\delta(\Delta\dot{\mathbf{p}}_w)$ contain the iterative corrections to the variables, while Φ_u and Φ_p are the residuals. The subscripts between parentheses denote the step of the iterative process, which is to be continued until a suitable tolerance criterion is fulfilled. Further details about the attainment of these equations can be found in Zienkiewicz et al. (1999).

Constitutive model: formulation of the rate dependent plasticity–viscoplasticity theory

Along with the mathematical and numerical models described so far, the third main ingredient for the numerical analysis of the landslide behaviour is the choice of an appropriate constitutive model for the materials. As pointed in the introduction, deep investigation of the Portalet landslide including remote sensing monitoring, in situ and laboratory tests as well as previous numerical simulations attempts indicate that viscous phenomena and delayed deformation due to creep plays a fundamental role in the landslide kinematics.

The concept of the viscoplastic model described in this section and used in the further simulations is based on Perzyna’s theory (1966). Perzyna’s theory is a modification

of classical plasticity wherein viscous-like behaviour is introduced by a time-rate flow rule employing a plasticity yield function. Similar to the rate-independent theory the strain rate is decomposed into an elastic and a viscoplastic strain rate:

$$\dot{\boldsymbol{\varepsilon}} = \dot{\boldsymbol{\varepsilon}}^e + \dot{\boldsymbol{\varepsilon}}^{vp} \quad (10)$$

The stress rate tensor $\dot{\boldsymbol{\sigma}}$ is related to the elastic strain rate via a constitutive tensor D_e , which is constant in the case of linear elasticity and variable (stress dependent) in the case of hypo or hyperelasticity:

$$\dot{\boldsymbol{\sigma}} = \mathbf{D}_e(\dot{\boldsymbol{\varepsilon}} - \dot{\boldsymbol{\varepsilon}}^{vp}) \quad (11)$$

In the theory proposed by Perzyna (1966), the viscoplastic strain rate is defined in a similar fashion as in the rate-independent plasticity theory:

$$\dot{\boldsymbol{\varepsilon}}^{vp} = \gamma\langle\phi(f)\rangle \frac{\partial g}{\partial \boldsymbol{\sigma}} \quad (12)$$

where γ is the fluidity parameter (which is the reciprocal of viscosity). $\langle\phi(f)\rangle$ is the viscous flow function, which represents the current magnitude of viscoplastic strain rate. g denotes the viscoplastic potential function and f any valid plasticity function playing the role of loading surface. A Mohr–Coulomb yield surface has been adopted for the failure criteria. Associative flow is invoked by $f=g$. $\frac{\partial g}{\partial \boldsymbol{\sigma}}$ represents the current direction of the viscoplastic strain rate. The viscous flow function is defined by:

$$\langle\phi(f)\rangle = \begin{cases} \phi(f) & , f > 0 \\ 0 & , f \leq 0 \end{cases} \quad (13)$$

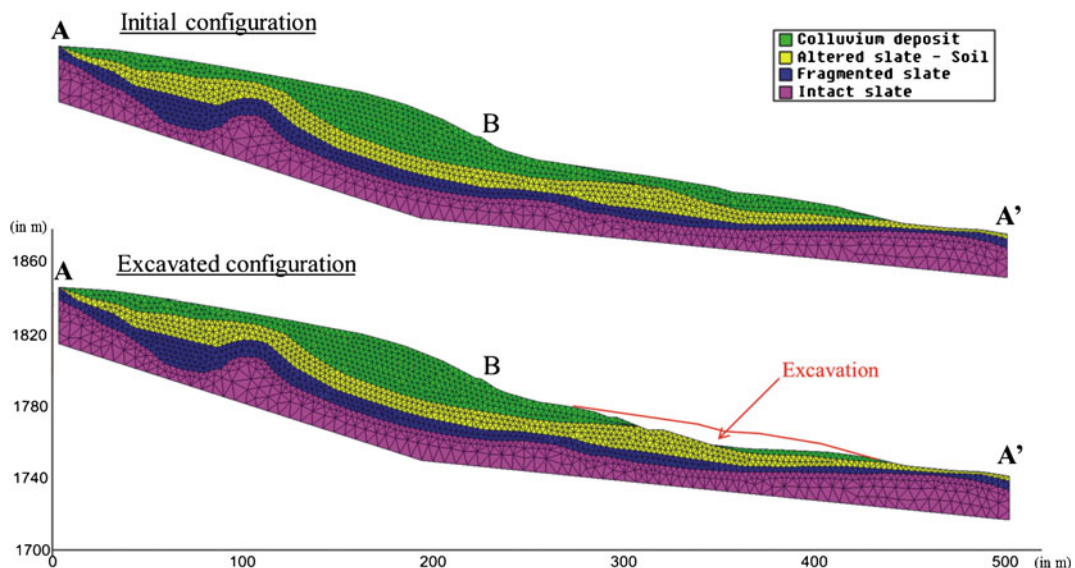


Fig. 5 Finite element mesh in the initial and excavated configuration

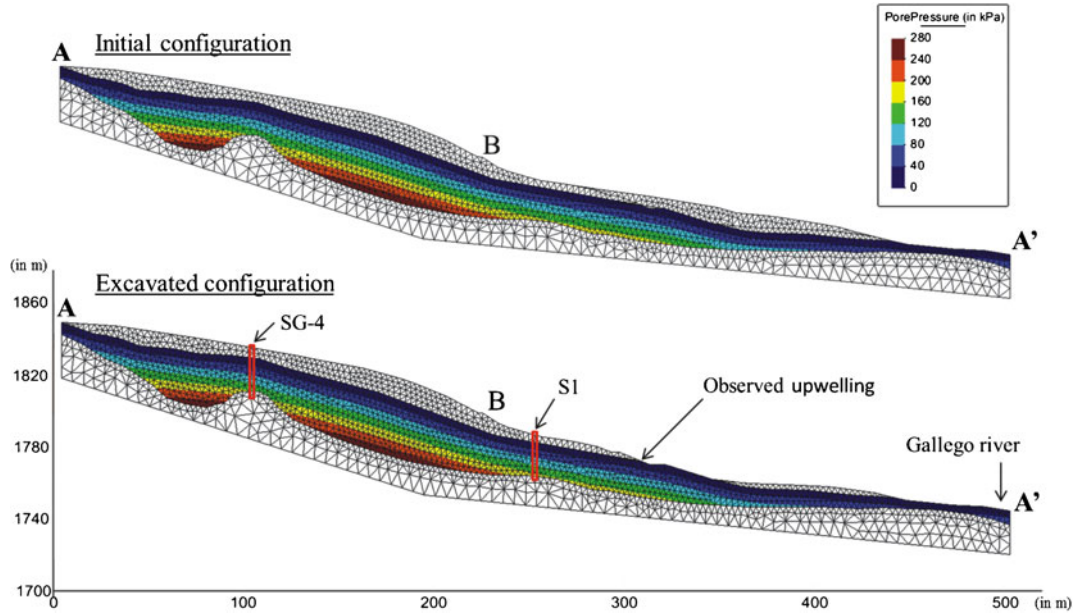


Fig. 6 Pore-pressure contours

where $\langle \rangle$ denotes Macauley brackets. A choice for the function ϕ is:

$$\phi = \left(\frac{f - f_0}{f_0} \right)^\alpha \quad (14)$$

in which α is a material constant. Concerning algorithm aspects, in displacement-based finite element formulations, stress updates take place at the Gauss points for a known nodal displacement. We start from time t_n with the known converged state: $[\epsilon_n, \epsilon_n^{vp}, \sigma_n, \kappa_n]$ (namely total strain, viscoplastic strain, stress and a scalar internal variable that characterises the size of the loading surface for the purpose of introducing hardening or softening behaviour) to calculate the corresponding values at time $t_{n+1} = t_n + \Delta t$: $[\epsilon_{n+1}, \epsilon_{n+1}^{vp}, \sigma_{n+1}, \kappa_{n+1}]$. In this incremental process, from Eqs. (10) and (11):

$$\Delta \epsilon = \epsilon^e + \Delta \epsilon^{vp} \quad (15)$$

$$\Delta \sigma = D_e (\Delta \epsilon - \Delta \epsilon^{vp}) \quad (16)$$

Therefore the key feature of the stress updates is characterised by estimating the incremental viscoplastic strain $\Delta \epsilon^{vp}$. Details of the numerical implementation can be found in the textbooks (Owen and Hinton 1986; De Souza Neto et al. 2008). It has to be noticed also that for softening problems the viscoplasticity approach has a regularizing effect in the sense that the initial-value problem remains well-posed avoiding instability due to strain and strain-rate softening (Wang et al. 1997).

Numerical simulations

This section presents the numerical simulations performed on the profile AA' of the Portalet landslide using the finite element code GeHoMadrid where the mathematical, constitutive and numerical models presented above have been implemented (Fernandez-Merodo 2001; Mira 2001).

The profile AA', defined in the geological sketch in Fig. 1, has been discretised using quadratic triangular elements. The mesh is composed by 3,594 triangles and 7,457 nodes. Initial and excavated configurations are presented in Fig. 5. Mesh size could be a restriction issue in terms of computing effort when we deal with simulations of non-linear dynamic problems. In this case, a typical time-dependent analysis of the Portalet landslide simulating the behavior of 8 years can be achieved in 9 h (CPU time using a single 3.33 GHz processor with 8 Gb of RAM).

The material parameters used in the simulations are obtained from in-situ and laboratory tests described in the geological description section (Table 1) taking into account the following assumptions: (1) the materials have a perfectly plastic behaviour following the Mohr-Coulomb criterion, (2) the flow is associative, (3) no softening is considered and (4) viscoplastic behaviour of the altered slate soil is taken into account in the transient analysis.

It has to be pointed out that the stratigraphy described in Fig. 5 and the material parameters given in Table 1 have been kept equal for

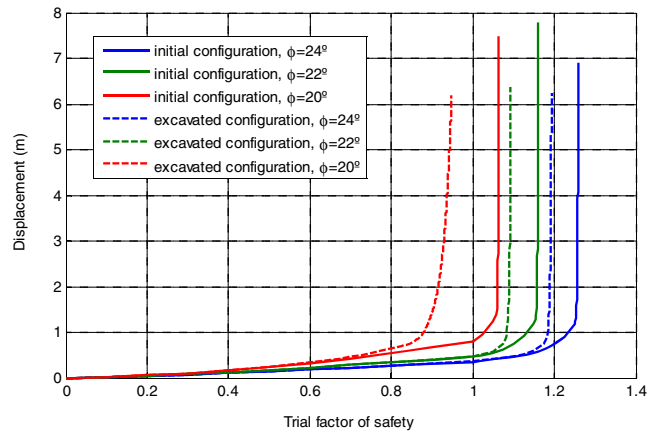
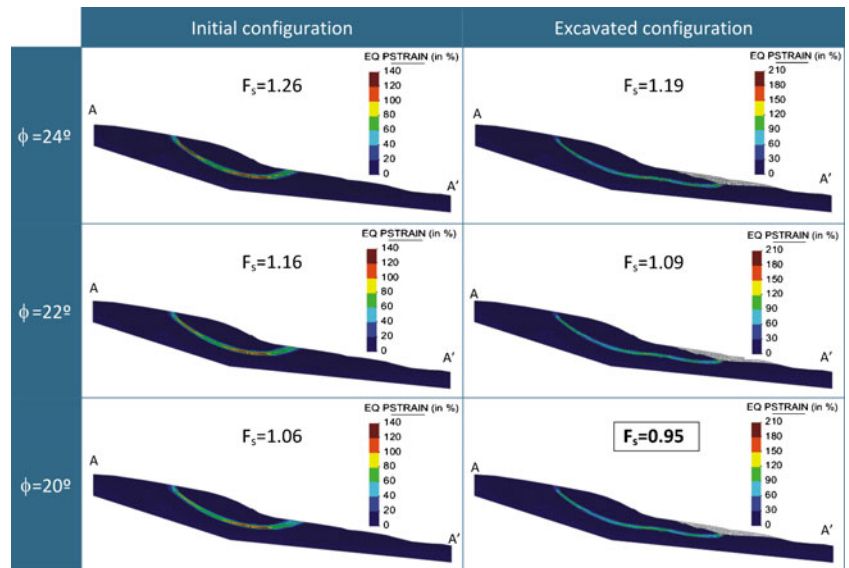


Fig. 7 Mid-slope horizontal displacement versus trial factor of safety

Fig. 8 Equivalent plastic strain contours at failure and associated factors of safety F_s



all the numerical simulations. We assume also that the bedrock limestone material and faults (Fig. 1) do not influence the landslide behaviour.

A previous stability analysis is performed on the initial and excavated configurations in order to determine sensitivity to parameter variations, and more precisely sensitivity to the friction angle of the altered slate soil. Its range has been estimated to be between 24° and 20° .

Ground water level position is also a critical factor on the slope stability. The observed upwelling of water on the excavated profile and in-situ ground water level position measurements in bore-holes SG-4 and S-1, reveal that the ground water level is 6.5 m deep, following the contact between the colluvium deposit and the altered slate material. These measurements coincide with the water level position estimated through back analysis modelling by Herrera et al. (2009) and Fernandez-Merodo et al. (2008). Note that in both previous works, no measurements about the real position of the water

level were available. The hydrostatic condition and the initial pore water pressure contours are sketched in Fig. 6. The transient response taking into account rain condition has been performed in the following time-dependent behaviour section.

Previous stability analysis

In order to evaluate the influence of the friction angle of the altered slate soil, a stability analysis has been performed on the initial and excavated configurations using the shear strength reduction method (Dawson et al. 1999). Figure 7 presents the solution of the stability analysis, plotting the horizontal displacement of point B located at mid-slope and defined in Fig. 5 versus the trial factor of safety F_s for different values of the friction angle ranging from 24° to 20° and keeping all the other material parameters constant (Table 1). It can be observed that the friction angle of the altered slate soil has an important influence on the stability analysis. Furthermore, when this friction angle is equal to 20° ,

Fig. 9 Left Equivalent plastic strain. Right Displacement contours after excavation

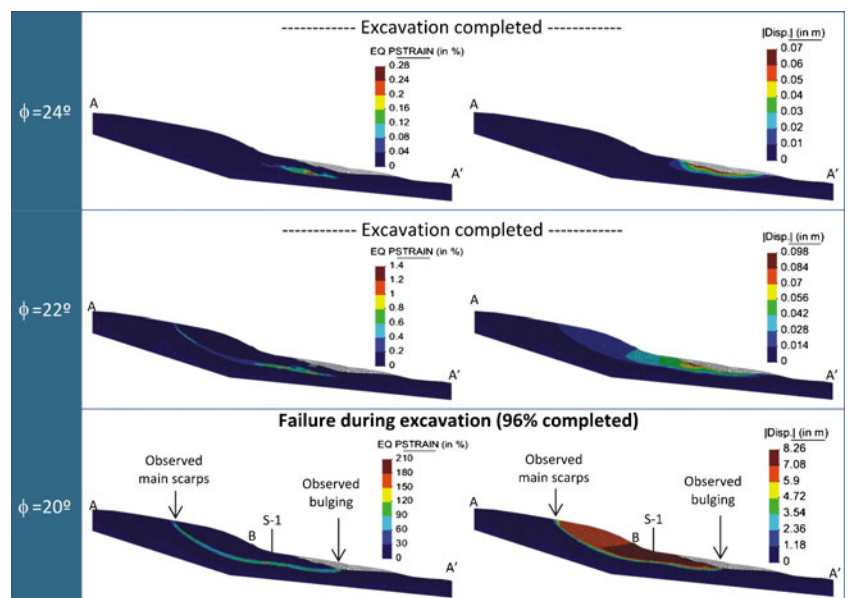
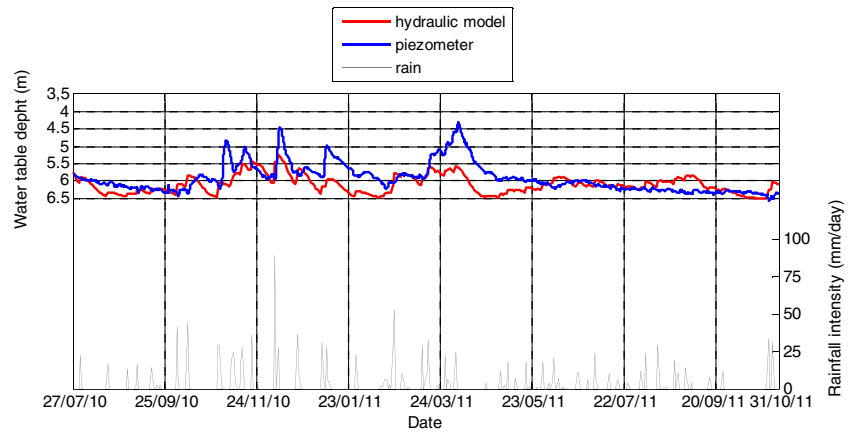


Fig. 10 Computed (red line) and measured (blue) water table depth, and rainfall intensity (gray) from 27/07/2010 to 31/10/2011



the initial configuration is stable ($F_s > 1$), whereas for the excavated configuration failure is reached ($F_s < 1$). Note that failure is reached when the horizontal displacement increases exponentially. Higher values of the friction angle yield stable condition for both configurations. Figure 8 presents the respective equivalent plastic strain contours at failure and associated factors of safety F_s . It has been cross-checked that this stability analysis gives identical results when we use standard limit equilibrium techniques. It also has to be pointed from a numerical point of view, the outstanding localisation of the computed shear zone as well as the big rate of achieved deformation. This is due to the performance of the GeHoMa-drid code: a smooth hyperbolic approximation of the Mohr-Coulomb yield criterion (Abbo and Sloan 1995), an implicit algorithm (Ortiz and Popov 1985) and a consistent tangent matrix (Simo and Taylor 1985) have been used to guaranty the quadratic convergence of the stress update algorithm.

The stability analysis yields an important result: the excavation can only be completed when the friction angle of the altered slate soil is higher than 20° . This result is verified when we proceed with a numerical simulation of the excavation. We start from the initial configuration in equilibrium (geostatic and hydrostatic equilibrium), then the excavated material is progressively removed using a static analysis. Figure 9 shows the equivalent plastic strain (second invariant

of the plastic strain tensor) and the displacement contours at the end of this excavation process for the different friction angle values. Note that both the plastic strain and the displacements are very small for $\phi = 24$ and 22° , affecting only the surrounding zone of the excavation. On the other hand for $\phi = 20^\circ$, failure occurs when 96 % of the excavation is completed. In this case, plastic deformation develops along a shear surface and the displacements contour indicates that the local excavation triggers a new landslide. In the bottom part of the Fig. 9, it can be appreciated that, according to the computations, the mobilised mass slides along this shear surface with a typical rigid-body motion (translational slide). It has to be underlined that computed location of the rupture surface agrees fairly well with field observations: The observed main scarps and bulging on profile AA' (Fig. 1 and 2) are located at the same position on the upper and lower part of the slope. Besides, the computed failure mechanism corresponds with the inclinometer measurements (Fig. 3). Moreover, the size of the computed mobilised mass coincides with the size and deformation patterns measured with ground based and satellite differential SAR interferometry (Fig. 4).

Hydraulic model

Previous works have shown that the Portalet landslide motion is influenced by rain infiltration and variations of the pore water

Fig. 11 Computed water table depth (red line) and rainfall intensity (gray) from 01/07/2004 to 31/10/2011

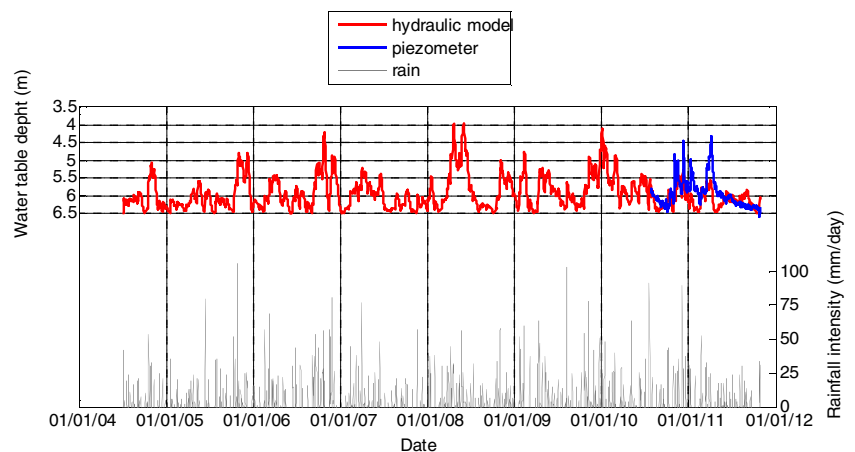
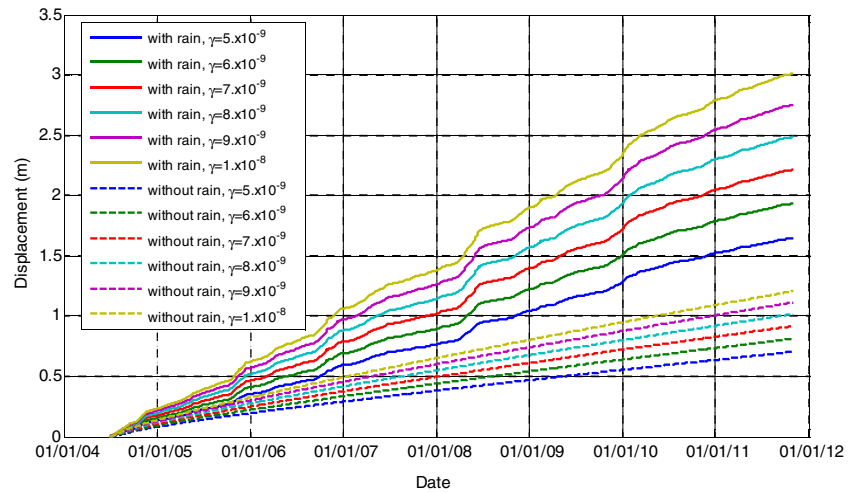


Fig. 12 Computed mid-slope horizontal displacement from 01/07/2004 to 31/10/2011 for different values of fluidity parameter γ (in $\text{Pa}^{-1}\text{s}^{-1}$) with and without rain action



pressure (Herrera et al. 2009, 2011). A full coupled hydro-mechanical finite element model was proposed in Fernandez-Merodo et al. (2008) where rain was modelled as an input flow condition on the upper boundary and taking into account water percolation through material permeability. In order to avoid model

uncertainties in the partially saturated zone we have used the simple hydraulic procedure described in Herrera et al. (2009).

In this case, the existing close relationship between landslide rate of displacement and rainfall suggests that it is possible to simulate the displacements from daily rainfall intensity instead of

Fig. 13 Computed and measured mid-slope horizontal displacement from 01/07/2004 to 31/10/2011

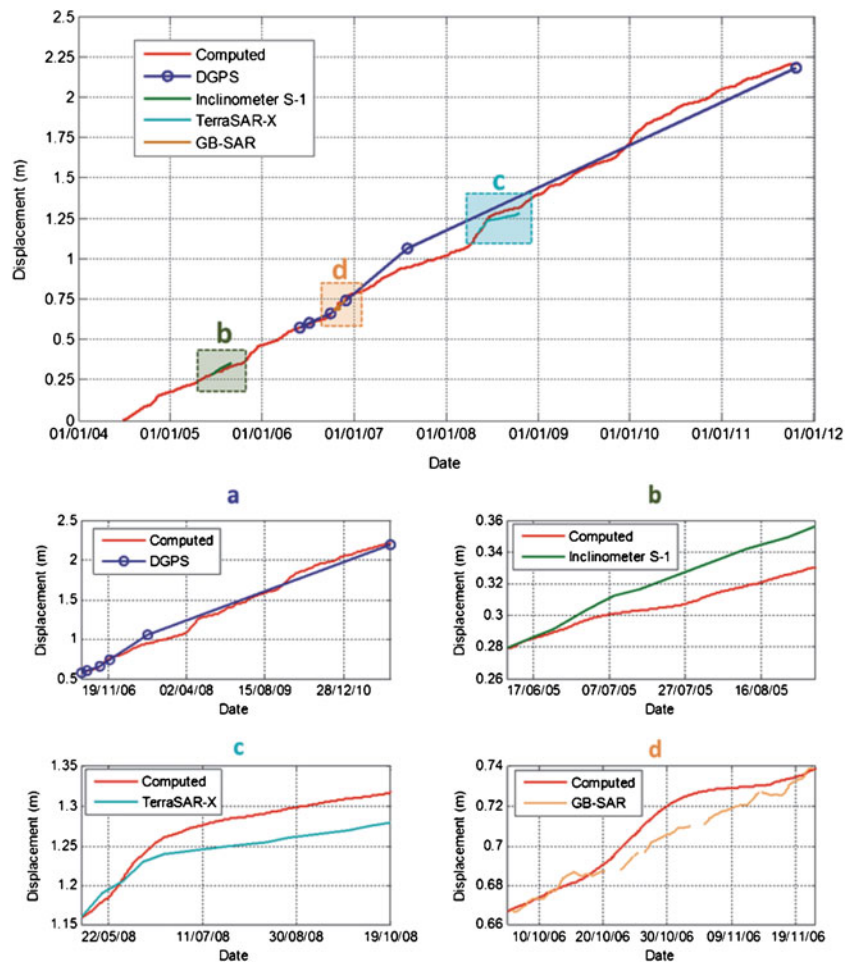
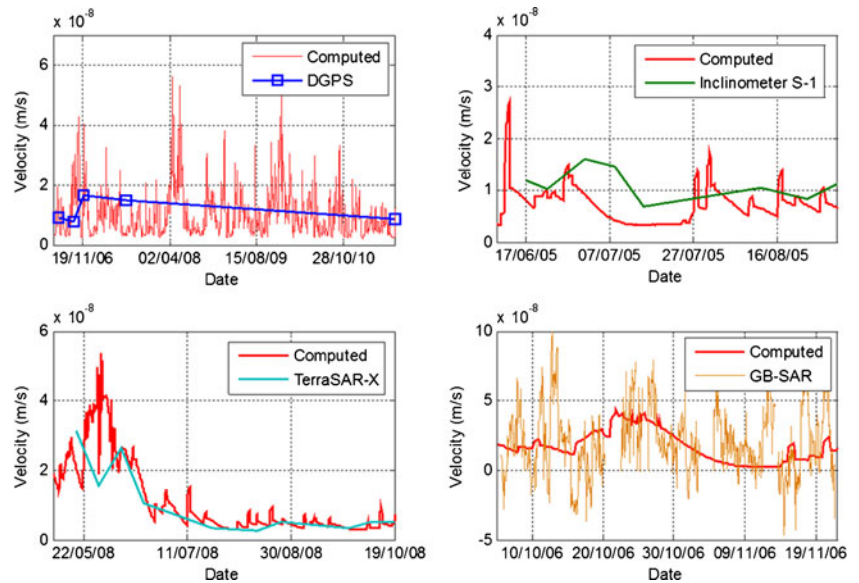


Fig. 14 Computed and measured mid-slope horizontal velocity from 01/07/2004 to 31/10/2011



groundwater level changes. Note that the effect of the snow melting during the spring season cannot be considered.

Measured displacements showed that the landslide reacts almost immediately to rainfall inputs. This rapid response is likely due to the drainage capacity of the colluvium deposit located on top and to the presence of superficial cracks and preferential drainage pathways. Changes in groundwater level have been considered directly proportional to the rainfall intensity through:

$$z_w = \frac{I_{\text{rainfall}}/1,000}{n} \quad (17)$$

where rainfall intensity I_{rainfall} (in $\text{mmm}^{-2}\text{day}^{-1}$) is divided by 1,000 to obtain groundwater level changes z_w (in m). n is the material porosity supposed to be constant and equal to 0.15 as proposed by Herrera et al. (2009). No runoff is contemplated when rainfall intensity exceeds the infiltration capacity and the material is supposed to be dry above the water table.

Even if it is not strictly a consolidation process, pore-pressure evolution in the landslide can be approximated by

the Terzaghi's one-dimensional consolidation theory. Assuming a parallel flow to the initial prescribed ground water level position, the dissipation of the excess pore-fluid pressure in a layer of length h_s is governed by:

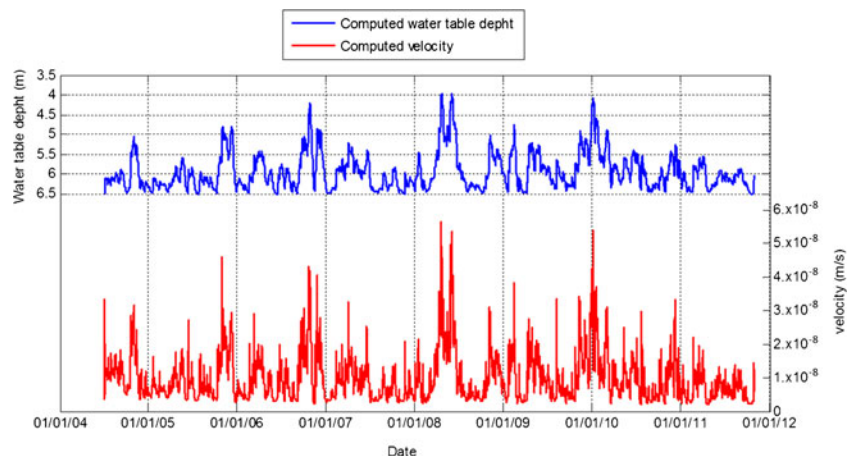
$$ep_w(t) = ep_{w0} \cdot e^{-\frac{t}{T_v}} \quad (18)$$

where ep_{w0} is the excess pore pressure ($ep_{w0} = z_w \cdot \gamma_w$, γ_w being the specific weight water), T_v is a time factor defined by $T_v = \frac{4h_s^2}{\pi^2 c_v}$ and c_v is the consolidation coefficient. T_v controls the dissipation time of the excess pore-fluid pressure.

This simple hydraulic model and the material parameter $T_v = 5 \times 10^6$ s selected in the original work (Herrera et al. 2009) can now be checked with the new available data recorded from the piezometer installed in July 2010. Figure 10 compares the water table depth given by the new piezometer and that computed by the hydraulic model from 27/07/2010 to 31/10/2011.

Error source of this hydraulic model include the 8 km distance to the Sallent de Gállego rain gauge station, evaporation, runoff and

Fig. 15 Computed mid-slope horizontal velocity (red line) and water table depth (blue) from 01/07/2004 to 31/10/2011



snow melting. Nevertheless, the solutions of this simple hydrological model approximate well the water table depth evolution measured by the piezometer. Taking into account the available rainfall intensity data, the water table depth variations is approximated from 01/07/2004 to 31/10/2011 (Fig. 11) that corresponds to the time-dependent behaviour period simulated in the next section.

Time-dependent behaviour

Time-dependent behaviour of the landslide is simulated from 01/07/2004 to 31/10/2011, which corresponds to the period from the parking excavation up to the last recorded measurements.

We take into account two factors for the time-dependent behaviour: the hydrological changes due to rain infiltration and the delayed viscoplastic behaviour of the altered slate material. Here, no strain softening and weathering processes is considered to simplify the problem.

The hydrological changes due to rainfall are prescribed as pore-pressure changes derived from the computed water table depth variations (previous section). Equivalent excess pore pressure is prescribed in all the landslide assuming a parallel flow to the initial prescribed ground water level position sketched in Fig. 6.

Viscoplastic behaviour of the altered slate material (level L2) is introduced using the proposed Perzyna theory for this material. The rest of the materials remains perfectly plastic using the same parameters (Table 1). The friction angle and the cohesion of the altered slate material (level L2) are deduced from the previous stability analysis, $\phi=20^\circ$ and $c'=10$ kPa, which correspond to an unstable state in the excavated configuration.

In order to evaluate the influence of the fluidity parameter γ , time dependent analysis has been performed using different values of γ with and without rain action. α in Eq. 14 has been kept constant and equal to one. Figure 12 shows the results of this analysis plotting mid-slope horizontal

displacement versus time.

A first interesting comment is that the viscoplastic behaviour allows constructing the parking even if the excavated configuration is not in equilibrium (see “Previous stability analysis”). Deformation is delayed in time and tends to infinity due to the failure state. Fluidity parameter controls the velocity of the delayed behaviour and rain infiltration accelerates the process.

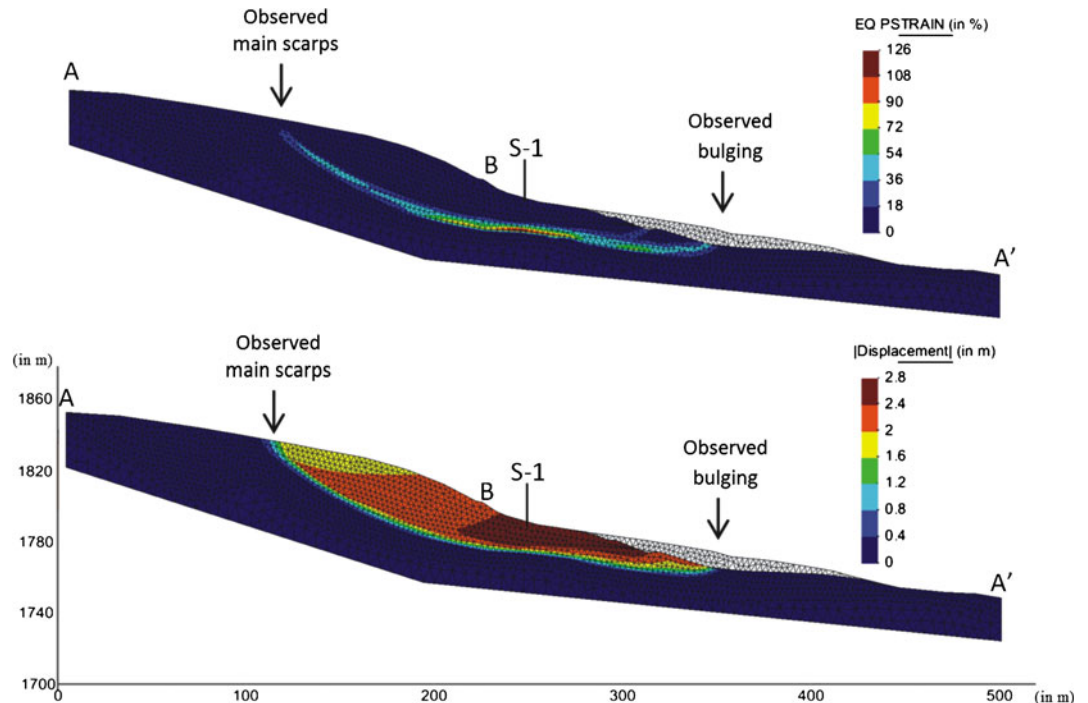
If $\gamma=7\times 10^{-9}\text{Pa}^{-1}\text{s}^{-1}$, the computed horizontal displacement at mid-slope fits reasonably well with the displacements measured in the monitoring campaigns (Fig. 13). A more precise comparison can be made if we plot the computed and measured mid-slope horizontal velocity in Fig. 14.

Figure 15 plots the computed mid-slope horizontal velocity and the computed water table depth evolution, showing that the landslide reacts directly to the water table changes. When the water depth is 6.5 m below the surface, the hydrostatic condition is verified nevertheless the landslide continues to move at $3\times 10^{-9}\text{m/s}$ due to the viscoplastic behaviour during the secondary creep.

Finally, equivalent viscoplastic strain (second invariant of the viscoplastic strain tensor) and displacement contours are checked at the end of the analysis in Fig. 16. As in “Previous stability analysis”, according to the computations, viscoplastic deformation develops along a shear surface and the mobilised mass slides along this shear surface with a typical rigid-body motion (translational slide). It has to be underlined the existing great correspondence between the computed failure mechanism and field observations, inclinometer measurements and SAR deformation patterns (Figs. 2, 3 and 4).

Therefore, through the implementation of this model, we have been able to reproduce the landslide mechanics that are responsible for measured ground surface displacements.

Fig. 16 Top Equivalent viscoplastic strain. Bottom Displacement contours at 31/10/2011



Discussion and conclusions

Slow landslides modeling is a challenge due to the three major factors that control the temporal evolution of landslides kinematics: (1) the pore-pressure fluctuations due to rain events and seasonal features (snow, dry season), (2) the shear strength reduction due to weakening and (3) the delayed displacement behaviour due to soil creep.

Complex numerical models as the finite element method can provide a good understanding of the mechanism of failure in these cases as they can correctly reproduce the fully coupled hydrogeological and mechanical behaviour. Moreover, advanced constitutive laws can be used. In this work, the time-dependent $u-p_w$ formulation beside a simplified groundwater model taking into account directly the recorded daily rainfall intensity and a viscoplastic model based on Perzyna's theory with a Mohr–Coulomb rupture criteria were used to model kinematics of the Portalet landslide.

Unlike the previous work performed in Portalet landslide (Herrera et al. 2009), no forecasting analysis has been carried out. In the former, it is a simple 1D approach, where very few parameters are needed to reproduce qualitatively and “quantitatively” the recorded motion. After calibrating the unknown model parameters by back analysis in a fixed period of time, the simple model can be used to predict the landslide mobility in another period of time. On the job at hand, the number of input parameters is greater, giving a more realistic, but more complex, spatial and temporal representation of the landslide. On the one hand, the proposed viscoplastic model reproduces the constant creep rate measured during the monitoring campaigns; on the other hand, the proposed coupled formulation reproduces acceleration and deceleration of the landslide when the water table rises and goes down, respectively. It should be recalled that this is an active landslide that has been reactivated after the 2004 excavation on the toe. After the constructive solutions were undertaken, the slope remains in an unstable situation ($F_s < 1$), and both the model and the monitoring data show a 2-m displacement in the past 8 years.

Three major sources of uncertainties result from the proposed model: the mechanical, hydraulic and viscosity parameters. The mechanical parameters are obtained from the performed in situ and laboratory tests, but they are not completely reliable in the colluvium and altered soil due to the heterogeneity of the grain size in the colluvium and the degree of alteration in the slate material. The hydraulic parameters and related water table evolution have been checked with a piezometer only available since July 2010. The viscosity parameters were obtained from back analysis; nevertheless, according to van Asch et al. (2007), there is a mismatch between values obtained from the ring shear laboratory test and those obtained from back analysis. Overall, the back analysis of the kinematic behaviour of large slow landslides is far from being a simple or trivial task if we take into account all these three aspects at once.

After a good calibration, the proposed model can give successful short-term and medium-term predictions during stages of primary and secondary creep, i.e. at nearly constant strain rate. However, long-time predictions remain uncertain. On the one hand, stability depends strongly on the position of the water table depth, a decrease in the pore pressure would slow down gradually the landslide and eventually stop it if the associated safety factor becomes higher than one, an increase in the pore pressure would accelerate the movement. On the other hand, new failures during tertiary creep due to soil temporal micro-structural degradation are still insufficient

understood and should be first observed and calibrated in long-term laboratory tests.

Acknowledgements

This work has been partially funded by the Terrafirma Global Monitoring for Environment and Security program from ESA, the project DO-SMS (SUDOE INTERREG IV B), the DORIS Project “Ground Deformation Risks Scenarios: an Advanced Assessment Service” (EU-FP7-SPACE-2009-1n 242212) and the Project SAFE-LAND “Living with landslide risk in Europe: Assessment, effects of global change and risk management strategies” (EU-FP7-ENV-2008-1 n 226479).

References

- Abbo AJ, Sloan SW (1995) A smooth hyperbolic approximation to the Mohr–Coulomb yield criterion. *Comput Struct* 54(3):427–441
- Álvarez-Fernández MI, González-Nicieza C (2011) Ensayos de hincamiento con cilindro hidráulico. Technical Report for Instituto Geológico y Minero de España. Control Remoto Sudoce Doris Project (in Spanish)
- ARCO TECNOS SA (2010) Sondeos en alrededores de la estación de Formigal (Huesca). Technical Report for Instituto Geológico y Minero de España. Control Remoto SudoceDorisProject (in Spanish)
- Bixel F, Muller J, Roger P (1985) Carte géologique du Pic du Midi d'Ossau et haut bassin du río Gállego, 1:25.000. Institut de Géodynamique, Université de Bordeaux, Bordeaux
- Cruden DM, Varnes DJ (1996) Landslide types and processes. In: Turner AK, Shuster RL (eds) *Landslides: investigation and mitigation*. Transportation Research Board, National Research Council, Special Report 247. National Academy Press, Washington, pp 36–75
- Dawson EM, Roth WH, Drescher A (1999) Slope stability analysis by strength reduction. *Geotechnique* 49(6):835–840
- De Souza Neto EA, Peric D, Owen DRJ (2008) *Computational methods for plasticity: theory and applications*. Wiley, Chichester
- Desai CS, Samtani NC, Vulliet L (1995) Constitutive modeling and analysis of creeping slopes. *J Geotech Eng, ASCE* 121(1):43–56
- Dounias GT, Potts DM, Vaughan PR (1988) Finite element analysis of progressive failure: two case studies. *Comput Geotech* 6:155–175
- Federico A, Popescu M, Fidelibus C and Interno G (2004) On the prediction of the time of occurrence of a slope failure: a review. In: *Proceedings 9th International Symposium on Landslides, Rio de Janeiro*, Taylor and Francis, London, vol. 2, pp 979–983
- Fell R, Hungr O, Leroueil S and Riemer W (2000) Keynote Lecture-Geotechnical engineering of the stability of natural slopes, and cuts and fills in soil, *GeoEng 2000, Vol.1, Invited Papers*, Technomic Publishing, Lancaster, pp.21–120
- Fernández-Merodo JA, Herrera G, Mira P, Mulas J, Pastor M, Noferini L, Mecatti D and Luzi G (2008) Modelling the Portalet landslide mobility (Formigal, Spain). *iEMSs 2008: International Congress on Environmental Modelling and Software*. Sánchez-Marré M, Béjar J, Comas J, Rizzoli A and Guariso G (eds) *International Environmental Modelling and Software Society (iEMSs)*
- Fernandez-Merodo JA (2001) Une approche à la modélisation des glissements et des effondrements de terrains: Initiation et propagation. Thèse de l'École Centrale Paris, no 2001–33 (in French)
- François B, Tacher L, Bonnard C, Laloui L, Triguero V (2007) Numerical modelling of the hydrogeological and geomechanical behaviour of a large slope movement: the Triesenberg landslide (Liechtenstein). *Can Geotech J* 44:840–857
- García Ruiz JM, Chueca J, Julián A (2004) Los movimientos en masa del Alto Gállego. In: Peña JL Longares L.A, Sánchez M (eds) *Geografía Física de Aragón. Aspectos Generales y Temáticos*, pp. 142–152.
- Herrera G, Fernández-Merodo JA, Mulas J, Pastor M, Luzi G, Monserrat O (2009) A landslide forecasting model using ground based SAR data: The Portalet case study. *Eng Geol* 105:220–230
- Herrera G, Notti D, García-Davalillo JC, Mora O, Cooksley G, Sánchez M, Arnaud A, Crosetto M (2011) Analysis with C-and X-band satellite SAR data of the Portalet landslide area. *Landslides* 8:195–206
- Leroueil S, Locat J, Vaunat J, Picarelli L and Faure R (1996) Geotechnical characterization of slope movements. In: Senneset K (ed) *Proceedings of the*

- Seventh International Symposium on Landslides, Trondheim, Norway, Balkema, Rotterdam, vol 1, pp.53–74
- Mira P (2001) Análisis por elementos finitos de problemas de rotura de geomateriales. Tesis Doctoral de la ETS de Ingenieros de Caminos, Canales y Puertos. Universidad Politécnica de Madrid (in Spanish)
- Ortiz M, Popov EP (1985) Accuracy and stability of integration algorithms for elastoplastic constitutive relations. *Int J Numer Methods Eng* 9:1561–1576
- Oviedo University (2011) Método y sistema para la realización de ensayos in situ y caracterización de terrenos heterogéneos o macizos rocosos intensamente fracturados. Spanish patent no ES-2351498-A1 (in Spanish). http://www.oepm.es/pdf/ES/0000/000/02/35/14/ES-2351498_A1.pdf. Accessed 27 Sept 2012
- Owen DRJ, Hinton E (1986) Finite elements in plasticity. Pineridge, Swansea
- Perzyna P (1966) Fundamental problems in viscoplasticity. *Rec Adv Appl Mech* 9:243–377
- Simo JC, Taylor RL (1985) Consistent tangent operators for rate independent elastoplasticity. *Comput Methods Appl Mech Eng* 48:101–118
- Tacher L, Bonnard C, Laloui L, Parriaux A (2005) Modelling the behaviour of a large landslide with respect to hydrogeological and geomechanical parameter heterogeneity. *Landslides* 2(1):3–14
- Troncone A (2005) Numerical analysis of a landslide in soils with strain-softening behaviour. *Geotechnique* 55(8):585–596
- Van Asch TWJ, Van Beek LPH, Bogaard TA (2007) Problems in predicting the mobility of slow-moving landslides. *Eng Geol* 91:46–55
- Varnes DJ (1978) Slope movement types and processes. In: *Landslides, analysis and control*. National Academy of Sciences, Nat. Res. Cou, Washington, Special Rep. vol 176, pp.11–33
- Vulliet L (2000) Natural slopes in slow movement. In: Zaman M, Booker JR, Gioda G (eds) *Modelling in geomechanics*. Wiley, Chichester, pp 654–676
- Wang WM, Sluys LJ, de Borst R (1997) Viscoplasticity for instabilities due to strain softening and strain-rate softening. *Int J Num Meth Eng* 40:3839–3864
- Zienkiewicz OC, Shiomi T (1984) Dynamic behaviour of saturated porous media: the generalised biot formulation and its numerical solution. *Int J Num Anal Meth Geomech* 8:71–96
- Zienkiewicz OC, Chan AHC, Pastor M, Shrefler BA, Shiomi T (1999) *Computational geomechanics with special reference to earthquake engineering*. Wiley, Chichester
- Zienkiewicz OC, Taylor R (2000) *The finite element method*, 5th edn. Butterworth-Heinemann, Oxford

J. A. Fernández-Merodo (✉) · **J. C. García-Davalillo** · **G. Herrera**

Geo-Hazards InSAR Laboratory, Geological Hazards Group,
Instituto Geológico y Minero de España,
c/ Ríos Rosas 23, 28003 Madrid, Spain
e-mail: jose.fernandez@igme.es

J. A. Fernández-Merodo · **P. Mira** · **M. Pastor**

M2i (Mathematical Modelling Engineering Group) Department of Applied Mathematics,
ETSI de Caminos, Canales y Puertos, UPM,
c/ Profesor Aranguren s/n, 28040 Madrid, Spain

J. C. García-Davalillo

Valencia Unit,
Instituto Geológico y Minero de España,
c/ Cirilo Amorós, 42, 46004 Valencia, Spain

P. Mira

Geotechnical Laboratory,
Centro de Estudios y Experimentación de Obras Públicas,
c/ Alfonso XII, 3 y 5, 28014 Madrid, Spain

P. Mira

Department of Civil Engineering,
EUIT de Obras Públicas, UPM,
c/ Alfonso XII, 3 y 5, 28014 Madrid, Spain